Supported VPO Catalysts for Selective Oxidation of Butane. II. Characterization of VPO/SiO_2 Catalysts

Kari E. Birkeland, Scott M. Babitz, Gregory K. Bethke, and Harold H. Kung*

Ipatieff Laboratory, Center for Catalysis and Surface Science, Northwestern University, Evanston, Illinois 60208

George W. Coulston

Central Research and Development Department, E.I. Dupont Company, Wilmington, Delaware 19880-0262

Simon R. Bare

Central Research and Development Department, Dow Chemical Company, Midland, Michigan 48674

Received: August 20, 1996; In Final Form: June 13, 1997[⊗]

SiO_2-supported VPO catalysts with different P/V ratios were prepared, used in selective oxidation of butane, and characterized by X-ray diffraction (XRD), laser Raman spectroscopy (LRS), near-edge X-ray absorption spectroscopy (XANES), and ^{31}P magic angle spinning NMR. Similar to the SiO_2-supported catalysts of lower metal loadings studied previously, the maleic anhydride selectivity increased with increasing P/V ratio, to greater than 50 mol % for P/V = 2. XRD and LRS detected predominantly α_1-$VOPO_4$ or a phase that is structurally very similar for both P/V = 1 and P/V = 2 samples. However, within the detection limit of the XANES experiment, the P/V = 1 catalyst contained mostly V^{5+} under reaction conditions, whereas the P/V = 2 catalyst contained 100% V^{4+}.

Introduction

Selective oxidation of butane to maleic anhydride is the only large scale commercial partial oxidation process which uses an inexpensive alkane for a direct feedstock. The commercial catalyst is bulk vanadium phosphorus oxide. In aged commercial catalysts, only vanadyl pyrophosphate ($(VO)_2P_2O_7$) is detected.[1,2] Nonetheless, on the basis of reports of surface P/V ratios substantially higher than unity[3−6] and the presence of V^{5+},[1,7,8] some investigators believe that a working catalyst contains more than one phase. While such claims of enrichment based on X-ray photoelectron spectroscopy studies may be incorrect,[9,10] there still is little agreement about the structure of the active surface.

In our effort to understand better the $(VO)_2P_2O_7$ catalyst, we synthesized supported VPO samples[11−13] with the hope that due to the higher dispersion of the active phase supported samples would be more amenable to generate information about the nature of the active surface. However, the use of a support also introduces support−oxide interactions that could affect the formation of the VPO phases. Indeed, reports in the literature all show much lower selectivity for maleic anhydride formation over supported as compared to unsupported VPO catalysts.[14−17] However, these reports did not provide sufficient information to understand the difference. Therefore, we have initiated a research program to characterize supported VPO catalysts to gain an understanding of the support effect and to determine the chemical properties important for high selectivity. In a previous report, we confirmed the literature results that the maleic anhydride selectivity for a SiO_2-supported VPO catalyst with a P/V ratio of unity was only about 30%.[11] However, one observation of great interest was that the selectivity increased with increasing P/V ratio and reached a plateau of about 50% for P/V ratios greater than 2. The samples produced X-ray diffraction (XRD) patterns of only the SiO_2 support due to the low loadings of V and P, but laser Raman spectroscopy (LRS) detected α_1-$VOPO_4$.

In order to better understand these supported catalysts, samples of SiO_2-supported VPO catalysts containing higher V and P loadings were prepared and characterized. In this paper, the results of characterization with ^{31}P magic angle spinning (MAS) NMR, LRS, XRD, and near edge X-ray absorption spectroscopy (XANES) are reported.

Experimental Section

Catalyst Preparation. Davisil silica, grade 644 or 646, was used as the support after the silica was washed in dilute nitric acid to remove trace Ca, Na, Ti, Al, Zr, and Fe impurities. A solution of ammonium metavanadate, oxalic acid, and dibasic ammonium phosphate of the desired P/V ratio was dissolved in deionized distilled water and was impregnated onto the silica by incipient wetness. The impregnated silica was air dried at 90 °C, calcined in air at 200 °C for 2 h, and then either calcined further at 520 °C for 6 h or activated directly in the reaction feed stream ($He/O_2/C_4H_{10}$ = 77/21/2) at 425 °C.

The compositions of the samples were determined by inductively coupled plasma−atomic emission spectroscopy. The samples are labeled as PV*n*, where *n* is the atomic P/V ratio, and their vanadium and phosphorus contents (wt %) were as follows. PV0: 6.8% V, 0% P. PV0.99: 6.54% V, 3.97% P. PV1.4: 6.43% V, 5.46% P. PV1.95: 6.28% V, 7.6% P. PV2.30: 6.21% V, 8.68% P. These values corresponded to the same V/Si ratio in every sample. The surface areas of the two most extensively characterized samples, PV0.99 and PV1.95, were 181 and 157 m^2/g, respectively.

The reference compounds, α_1-$VOPO_4$,[18,26] $VOPO_4 \cdot 2H_2O$,[18] $VO(PO_3)_2$,[19] and $(VO)_2P_2O_7$,[20] were prepared according to the methods in the literature.

Characterization. Steady-state butane oxidation was performed in a fused silica microreactor at near atmospheric

[⊗] Abstract published in *Advance ACS Abstracts,* August 1, 1997.

S1089-5647(96)02571-0 CCC: $14.00

TABLE 1: Dependence of Catalytic Properties of PV0.99 in Butane Oxidation on the Activation Conditions[a]

activation cond[b]	cat. wt (g)	flow rate (mL/min)	% butane conv	activity (mol C_4/mol V-min)	% selectivity				
					CO	CO_2	MA[c]	oxy[d]	crack[e]
air	0.100	51	9	0.029	52	19	26	2	1
air	0.202	25	25	0.020	55	21	21	1	2
rxn	0.152	99	11	0.046	49	17	29	3	1
rxn	0.152	50	20	0.042	51	18	28	2	1

[a] Reaction conditions: $He/O_2/C_4H_{10} = 77/21/1$, 375 °C. [b] Air: 2 h at 200 °C and 6 h at 520 °C. Rxn: activate directly in a reaction feed mixture at 425 °C. [c] Maleic anhydride. [d] Acrylic and acetic acids. [e] Ethene and propene.

pressure. Typically, reaction runs were made with a $He/O_2/C_4H_{10} = 77/21/2$ mixture at 375 °C, using 25 to 200 mL/min total flow rate and 0.05−2 g of catalyst sandwiched between plugs of acid-washed quartz wool. Fused silica chips were used to fill the reactor volume to minimize gas phase reactions. No detectable reaction was observed in the absence of a catalyst. The temperature of the catalyst bed was monitored with a thermocouple placed in a thermal well inserted in the catalyst bed. The reaction products were analyzed by gas chromatography using a combination of columns: a carbosphere column (6 ft × 1/8 in., 80/100 mesh, Alltech, room temperature) to separate O_2 from CO; a VZ-7 column (20 ft × 1/8 in., 60/80 mesh, Alltech, room temperature) to separate CO_2 from CO and O_2, and butane from butenes and butadiene; and a 5 wt % Carbowax on Graphpac GB column (25 ft × 1/8 in., Alltech, temperature programmed from 70 to 200 °C in five steps) to separate the oxygenates.

Laser Raman spectra were collected using the spectrometer described previously.[21] An Ar ion laser with 514.5 nm excitation wavelength was used. The spectra were collected in a controlled atmosphere cell. Typically, each sample was exposed to the reaction mixture at room temperature, heated to 375 °C, allowed to equilibrate, and then cooled back to room temperature in the reaction mixture. Spectra were collected both at 375 °C and at room temperature.

X-ray diffraction patterns were collected from catalyst wafers which contained an internal LiF standard, using Cu $K\alpha_{1,2}$ radiation and a Ni filter, on a Rigaku powder diffractometer. Diffraction peaks were fitted via nonlinear least square calculations. In situ vanadium K-edge XANES data were collected at the energy dispersive beam line X6A at the National Synchrotron Light Source, Brookhaven National Laboratory.[22] The data were recorded in the transmission mode using pressed wafers of optimum thickness in a Lytle-designed sample cell.[23] The data were recorded with no X-ray beam (the dark current signal, Dark), with the beam passing through the sample (Sample), and with the beam passing through a reference material (A1 foil, Ref). The normalized absorption was calculated using the equation:

$$\mu x = \ln[(\text{Ref} - \text{Dark})/(\text{Sample} - \text{Dark})]$$

where μ is the elemental absorption coefficient and x is the sample thickness. Typically, individual 20 ms scans were summed over a 2 s period. The reaction products were analyzed with an on-line mass spectrometer. Energy calibration was performed using a vanadium foil. All the XANES spectra were background subtracted with a linear function in the energy range 4900−4945 eV and subsequently normalized to unity in the continuum using the Macintosh edition of the University of Washington extended X-ray absorption fine structure analysis package[24] in order to make a meaningful comparison of the pre-edge features.

^{31}P magic angle spinning solid state NMR spectra were recorded on a 300 MHz Varian VXR300 spectrometer operating at 121.405 MHz with a Doty Scientific Inc. 5 mm supersonic cross-polarization MAS triple-tuned rotational echo double-resonance probe and SiN 5 mm rotors with vespel caps. A spinning rate of 10−11 KHz, a pulse width of 20 ms, and a delay time of 5 s between scans were used. Typically, 1800 scans were collected. 85% H_3PO_4 was used as the reference. The samples were pretreated in a U-tube microreactor in air at 300 °C or in a He/O_2/butane = 77/21/2 mixture at 400 °C for at least 2 h. After cooling to room temperature in the pretreatment gas stream, the samples were transferred to a dry bag without exposure to air, where the samples were loaded into the rotor and capped.

TABLE 2: Dependence of Catalytic Properties on the P/V ratio[a]

catalyst	activity (mol C_4H_{10}/min-mol V)	% C_4 conv	% selectivity				
			CO	CO_2	MA	oxy[c]	crack[d]
PV0	0.002	16	60	34	1	4	1
PV0.99	0.021	13	54	21	22	2	1
PV0.99	0.019	24	55	21	21	2	1
PV1.40	0.012	12	42	12	42	2	1
PV1.40	0.009	19	43	14	41	2	1
PV1.95	0.004	12	28	11	56	4	2
PV1.95	0.002	22	33	12	52	2	2
PV2.30[b]	0.001	3	38	14	51	0	0
α_1-$VOPO_4$		15	54	19	22	4	1

[a] Reaction condition: $He/O_2/C_4H_{10} = 77/21/2$, 375 °C. [b] Feed composition: $He/O_2/C_4H_{10} = 88/8/4$. [c] Acetic and acrylic acid. [d] Ethene and propene.

Results

Butane Oxidation. The dependence of butane oxidation selectivity and activity on activation condition and P/V ratios were examined. The relationship between activation condition and activity and selectivity is reported in Table 1. Both the activity and selectivity for maleic anhydride were slightly higher for the sample activated in the reaction mixture than that in air. The selectivity was only a weak function of butane conversion, decreasing from 35 to 28% as the conversion increased from 4 to 20% (figure supplied as Supporting Information). However, the P/V ratio exerted a much greater influence. As shown in Table 2, the selectivity increased as the P/V ratio increased up to 2, whereupon a value over 50 mol % maleic anhydride was achieved. However, the activity decreased beyond P/V = 1. This behavior resembled that observed for samples containing lower metal loadings.[11]

Because the P/V ratio in the unsupported catalyst is close to unity, whereas that for the SiO_2-supported sample of the highest maleic anhydride selectivity was 2, the samples PV0.99 (in some cases PV0.95) and PV1.95 were chosen for extensive characterization.

Raman Spectroscopic and X-ray Diffraction Characterization. The Raman spectra of sample PV0.99 were collected in a reaction mixture at 375 °C and after cooling to room temperature. The results are shown in Figure 1. These spectra were compared with the spectra of α_1-$VOPO_4$ (spectrum 1e)

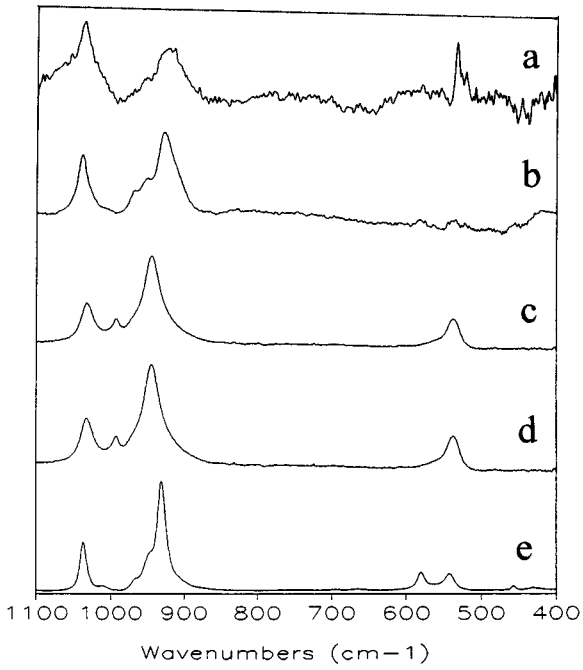

Figure 1. In situ Raman spectra of PV0.99 in $He/O_2/C_4H_{10} = 89/10/1$ at (a) 380 °C and (b) after cooling to room temperature. The spectra of (c) hydrated PV0.99, (d) $VOPO_4 \cdot 2H_2O$, and (e) α_1-$VOPO_4$ were collected at ambient conditions.

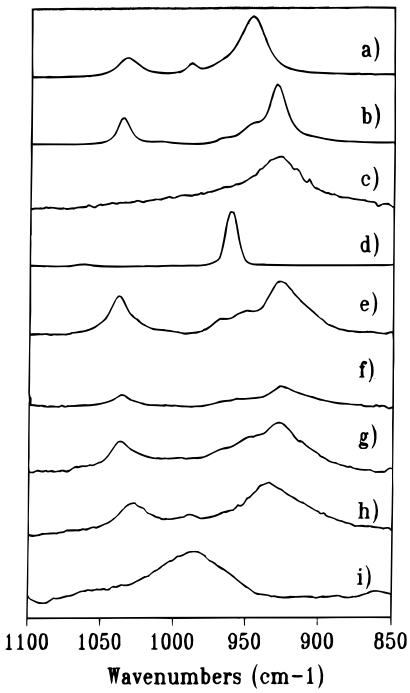

Figure 2. Raman spectra of (a) $VOPO_4 \cdot 2H_2O$ and (b) α_1-$VOPO_4$, collected at ambient conditions, and (c) poorly crystalline $(VO)_2P_2O_7$, (d) $VO(PO_3)_2$, (e) PV0.99, (f) PV1.4, (g) PV1.95, (h) PV2.4, and (i) dry 4.32 wt % P/SiO_2, collected after activation in a reaction mixture in the Raman cell and cooling to room temperature.

and $VOPO_4 \cdot 2H_2O$ (spectrum 1d), the latter being the hydrated form of α_1-$VOPO_4$. The spectra of α_1-$VOPO_4$ and $VOPO_4 \cdot 2H_2O$ were similar to those reported by Benabdelouahab et al.[25] The small band at 1009 cm^{-1} has been attributed to $VOPO_4 \cdot H_2O$.[26] Except for some peak broadening, the spectrum of PV0.99 collected at room temperature (spectrum 1b) closely resembled the α_1-$VOPO_4$ spectrum. The main features were retained even at reaction temperature (spectrum 1a). Storing the PV0.99 sample in a high-humidity atmosphere (spectrum 1c) hydrated the sample and yielded a spectrum characteristic of $VOPO_4 \cdot 2H_2O$.

The Raman spectra of SiO_2-supported samples with different P/V ratios, collected after the samples were cooled to room temperature in a reaction mixture, are reported in Figure 2, together with the spectra of reference compounds. The spectrum of $VO(PO_3)_2$ resembled the reported one.[27] The spectrum of $(VO)_2P_2O_7$ was characteristic of a poorly crystalline $(VO)_2P_2O_7$ sample.[25] Crystalline $(VO)_2P_2O_7$ has peaks at 933 and 921 cm^{-1}.[25] The PV/SiO_2 materials of all phosphorus loadings produced similar Raman spectra. However, with increased P loading, the (PO_4) symmetric stretch band at 930 cm^{-1} broadened and became less well defined and a shoulder at 910 cm^{-1} emerged. The supported samples probably did not contain α_{II}-, β-, δ-, or γ-$VOPO_4$ because the characteristic peaks in the 1050−1100 cm^{-1} region were absent.[25]

The XRD patterns of PV0.99 as prepared, post-reaction, and hydrated were obtained (supplied as Supporting Information). The silica support and the mounting slide material yielded broad diffraction envelopes centered at 12° and 22° 2θ. The hydrated sample had strong peaks at 12.41, 24.58, and 28.84°, and weak peaks at 32.80, 37.80, 41.10, 46.03, 46.37, 46.72, 51.37, 59.36, 59.89, 63.28, 65.50, and 67.16° 2θ. The peaks were too broad and weak to definitively assign the pattern to a given phase. However, the majority of these peaks were consistent with either $VOPO_4 \cdot 2H_2O$ or a mixture of $VOPO_4 \cdot 2H_2O$ and α_1-$VOPO_4$. The interlayer d spacing in the hydrated $VOPO_4$ material depends on the extent of hydration. The d spacing of the (001) plane shifts from 7.40 to 6.29 and 4.11 Å, resulting in a shift of the (001) diffraction from 11.94 to 14.06 and 21.62° 2θ (Cu $K\alpha_{1,2}$) for $VOPO_4 \cdot 2H_2O$, $VOPO_4 \cdot H_2O$, and α_1-$VOPO_4$, respectively. The observed shift of the (001) and (002) peaks in the PV0.99 material to 12.41 and 24.58 as compared to 11.94 and 24.02 for $VOPO_4 \cdot 2H_2O$ is consistent with incomplete hydration.

The air-calcined and reaction-used PV0.99 produced identical diffraction patterns. The two strongest features at 28.88 and 59.58° 2θ indexed well with the (200) and (400) diffractions of α_1-$VOPO_4$, respectively. However, the remaining peaks were shifted to slightly smaller d spacings. A lattice contraction along the *c* direction for a material with *P*4/*n* symmetry would cause all diffraction peaks with $l \neq 0$ to shift to higher angles. The X-ray powder pattern for a material in the *P*4/*n* space group, with the unit cell parameters $a = b = 6.20$ Å, and $c = 3.94$ Å (cf. $c = 4.11$ Å in α_1-$VOPO_4$), and the atom positions defined for a α_1-$VOPO_4$ structure provided peak positions corresponding to the supported PV sample. The 28.89, 41.70, 46.03, 54.76, 59.95, 63.58, and 67.45° 2θ peaks were assigned to the (200), (220), (002), (202), (400), (222) and/or (401), and (420) diffractions, respectively, for a α_1-$VOPO_4$ structure with a 0.17 Å contraction along the *c* direction. However, the relative peak intensities between XRD patterns generated from the proposed structure and the collected spectra remained somewhat different. Preferred orientation or slight changes in the vanadium position along the *c* direction could have caused changes in the relative peak intensities. The PV0.99 and PV1.95 samples produced virtually identical XRD patterns (supplied as Supporting Information).

XANES Characterization. The X-ray absorption edge and pre-edge positions of vanadium of different oxidation states were determined using reference compounds. Figure 3 contains representative XANES spectra for VPO phases containing vanadium oxidation states ranging from 3 to 5. From these spectra, the positions of the pre-edge absorption due to the 1s−3d transition were determined to be 5468.9, 5469.0, and 5470.9 eV, respectively, for oxidations states 3, 4, and 5, and

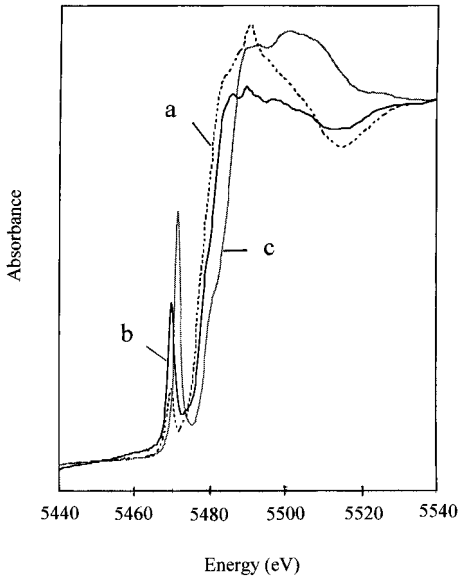

Figure 3. XANES of reference compounds: (a) $VOPO_4$, (b) $(VO)_2P_2O_7$, and (c) β-$VOPO_4$.

5469.7, 5478.7, and 5482.0 eV, respectively, for the inflection point of the K-edge absorption.

The spectra for the PV0.99 and PV1.95 samples collected under reaction conditions at 321 °C are reported in Figure 4, and those collected in a flow of 20% O_2 in He at the same temperature are reported in Figure 5. These spectra were curve-fitted using the average peak positions and full width at half-maximum (fwhm) determined from the reference compounds in Figure 3 and other vanadium phosphate phases. The position of the V^{5+} pre-edge transition and fwhm were set at 5470.9 and 2.60 eV, respectively, whereas those for V^{4+} were allowed to vary slightly to obtain the best fit. Three peaks above the absorption edge in the region 0−50 eV were used to obtain a better fit of the absorption edge position in the spectra of both the reference samples and the supported catalysts. The positions of these three peaks were not fixed, but they only varied over a small energy range in the final fits. The peak at about 20 eV above the absorption edge has been assigned as the dipole-allowed, 1s−4p transition.[28] These spectra could be fitted well without any contribution from V^{3+}. The parameters used to fit the spectra in Figures 4 and 5 are listed in Table 3.

From the results of curve fitting, the PV0.99 sample in O_2 was estimated to contain 100 ± 2% V^{5+}. From the change in the V^{5+} peak area and assuming that the relative concentrations of the vanadium species in a given sample under different treatment conditions were directly proportional to the area of the pre-edge absorption peak, the relative V^{5+} and V^{4+} concentrations in PV0.99 under reaction conditions were estimated to be 93 and 7%, respectively. Likewise, the PV1.95 sample was estimated to contain 100% V^{4+} under reaction conditions and, from the changes in the V^{4+} peak area, to contain 88% V^{4+} and 12% V^{5+} in O_2.

^{31}P MAS NMR. The ^{31}P MAS NMR spectra of a 0.83 wt % P/SiO_2 sample are supplied as Supporting Information. Similar to the literature results,[29] the P/SiO_2 sample produced four peaks at 1.6 (Q^0), −11.1 (Q^1), −23.9 (Q^2), and −37.1 (Q^3) ppm (referenced to 85% H_3PO_4), which have been assigned to P in O═P(OH)$_3$, O═P(OSi or P)(OH)$_2$, O═P(OSi or P)$_2$(OH), and O═P(OSi or P)$_3$, respectively. The relative intensities of these peaks depended on the degree of sample hydration. As expected, dehydration increased the intensities of the peaks with fewer hydroxyl groups. Similar observations were made with a 3.9 wt % P/SiO_2 sample.[13]

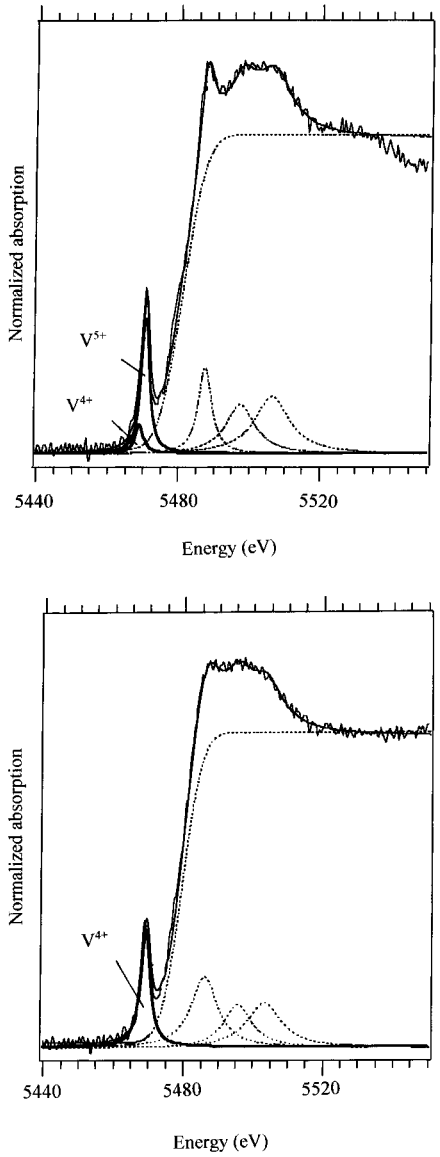

Figure 4. XANES spectra collected under steady-state butane oxidation conditions ($He/O_2/C_4H_{10}$ = 89/10/1 at 321 °C) for (a) PV0.99 and (b) PV1.95. The fitted spectra are also shown.

The spectrum of reaction-used PV0.95 is reported in Figure 6. The spectrum could be fitted well with peaks with the parameters listed in Table 4. Heating the sample in air at 310 °C for 3 h eliminated the broad peak at 27.1 ppm (Figure 7). Thus, as Vedrine and co-workers have proposed,[5] P interacting with a small amount of material that contained V^{4+} and V^{5+} ions probably produced this feature. Although the relative intensities of the peaks at −10.5, −23.4, and −38.6 ppm were in line with those for P/SiO_2, the peak at 3.5 ppm was proportionally too large to be attributed to P/SiO_2 entirely.

In order to avoid complications originating from paramagnetic V^{4+} ions, the spectrum of the air-calcined PV0.95 sample (Figure 7) was used to estimate the extent of phosphorus segregation between the silica surface and the vanadium phosphorus oxide phase. The values used in these calculations are listed in Table 5. If one assumed that the relative intensities of the four P on SiO_2 peaks were similar to those of the dehydrated P/SiO_2 sample, the P/SiO_2 contribution to the 3.5 ppm peak could be subtracted off. The remaining peak would still represent the majority of the P species in the spectrum. We have determined that bulk α_1-$VOPO_4$ yielded a sharp peak at 2.8 ppm, and $VOPO_4 \cdot 2H_2O$ at 8.1 ppm. These positions were similar to the reported 2.7 ppm for α_1-$VOPO_4$, 3.9 ppm for

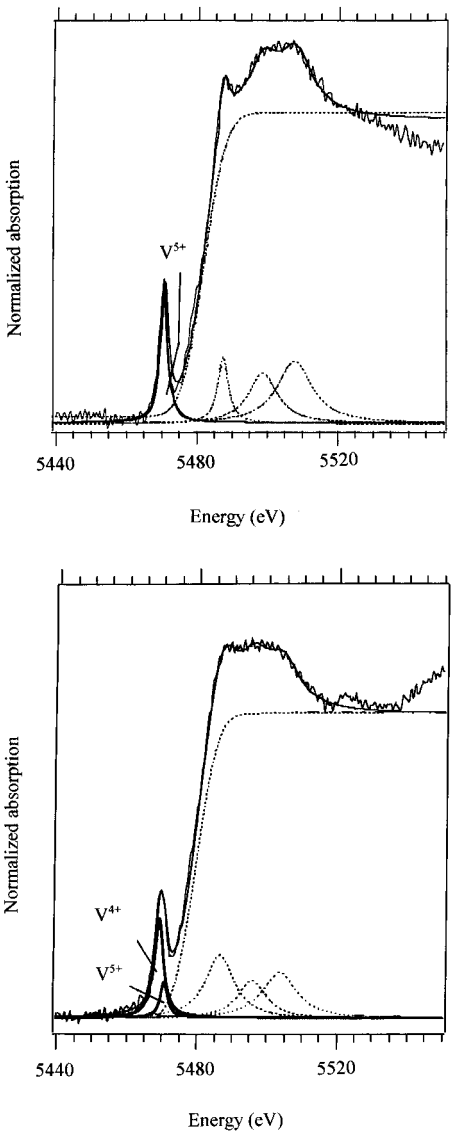

Figure 5. XANES spectra collected in 20% O_2 in He at 321 °C for (a) PV0.99 and (b) PV1.95. The fitted spectra are also shown.

$VOPO_4 \cdot H_2O$, and 6.6 ppm for $VOPO_4 \cdot 2H_2O$.[30] Considering the Raman and XRD data on the PV0.99 sample, the 3.5 ppm peak was attributed to a structure similar to α_1-$VOPO_4$, although its position was closer to that expected from $VOPO_4 \cdot H_2O$. Since the Q^0 P/SiO_2 peak was not resolved from the 3.5 ppm peak of α_1-$VOPO_4$, it was assumed that this sample had a Q^0/Q^1 ratio similar to the dry $P0.83/SiO_2$ sample. Then, the peak area of Q^0 in this sample could be estimated by

$$Q^0 \text{ area in PV0.95} = (Q^1 \text{ area in PV0.95})\,(Q^0 \text{ area in dry } P0.83/SiO_2 \div Q^1 \text{ area in dry } P0.83/SiO_2)$$

If one assumed that the spectrum represented all of the P in this sample, the percent of P interacting with silica and not vanadium could be estimated as follows:

$$\%\ P/SiO_2 \text{ in PV0.95} = 100[(Q^0 + Q^1 + Q^2 + Q^3)/(\text{total peak area})] = 19.1\%$$

That is, about 19% of the P existed as P/SiO_2, and 81% was associated with V. If all of the V in the sample was associated with P, the P/V ratio in the VPO species would be 0.81.

The ^{31}P MAS NMR spectrum of reaction-used PV1.95 is reported in Figure 8. The spectrum could be fitted with the parameters shown in Table 6. Similar to the spectrum of PV0.95 sample, the peaks at −10.6, −23.1, and −36.4 ppm could be assigned to P on SiO_2 and the peak at 3.2 ppm to a combination of P/SiO_2 and α_1-$VOPO_4$. If the same procedure was used as for the PV0.95 sample to estimate the amount of P segregated to the silica surface, and assuming that all of the V was associated with P, the average P/V ratio of the VPO species would be 1.77. The peak at 27 ppm was assigned to P interacting with a mixed V^{4+}/V^{5+} material. Consistent with the XANES results, the relative area under this peak was much larger for this sample than that for PV0.95.

The assignment of the 6.9 ppm peak in PV1.95 and the 6.4 ppm peak in PV0.95 was less definitive. Other P/SiO_2 species did not produce these features, because peaks at these positions were not observed for any of the P/SiO_2 samples. However, they might have originated from $VOPO_4 \cdot 2H_2O$, which has a peak between 6.6 and 8.1 ppm. Alternatively, they might have originated from small changes in the local P environment within the supported VP oxide. Cheetham and co-workers have proposed that correlations between bond strengths at the phosphate oxygen atoms and the ^{31}P isotropic chemical shift form a basis both for structural analysis and peak assignments in phosphate materials.[31] Thus, the 6.9 and 6.4 ppm features might represent an interaction of P with V^{5+} that results in a weaker total bond strength at the phosphate oxygen atoms than that observed in α_1-$VOPO_4$. These features will be further discussed later.

Discussion

Catalytically, the current series of samples behaved similarly to the earlier series that contained lower metal loadings.[11] However, the higher loadings facilitated catalyst characterization. The discussion here will concentrate on the structure of the supported VPO phases and the oxidation state of V.

The VPO phases detected by Raman spectroscopy and XRD were based structurally on α_1-$VOPO_4$. The Raman spectrum of PV0.99 was the same as that for bulk α_1-$VOPO_4$. With increased phosphorus loading, the band for the (PO_4) symmetric stretch at 930 cm^{-1} broadened and became less well defined (Figure 2). The XRD patterns for PV0.99 and PV1.95 were virtually identical and indexed well to a proposed structure based on α_1-$VOPO_4$ with a lattice contraction along the *c* direction from 4.11 to 3.96 Å. Because the XRD patterns did not change with phosphorus loading, either the phosphorus formed a material without sufficient long range order to be detected with XRD or the phosphorus substituted into α_1-$VOPO_4$ (with contraction along the *c* direction) without altering the *a* and *b* lattice parameters.

XANES analysis indicated that the PV0.99 and PV1.95 samples contained 7 ± 2% and 100 ± 2% V^{4+}, respectively, under reaction conditions (in a $He/O_2/He$ = 89/10/1 stream at 321 °C). Thus, phosphorus enrichment stabilized V^{4+} and promoted higher maleic anhydride selectivity.

^{31}P MAS NMR provided information of the phosphorus environment in the samples. Phosphorus both modified the silica surface to form O═P(OSi or OP)$_x$(OH)$_{3-x}$ species and the vanadia to form silica-supported vanadium phosphorus oxide species. Therefore, the P/V ratios calculated from inductively coupled plasma analyses overestimated the P/V ratio of the VPO species. For the PV0.99 and PV1.95 samples, the P/V ratios of the VPO species were at most 0.77 and 1.77, respectively.

PV1 Samples. For samples of P/V = 1 (PV0.99 and PV0.95), the Raman and ^{31}P MAS NMR data are consistent

TABLE 3: Parameters Used to Fit the XANES Spectra of PV0.99 and PV1.95 Samples[a]

		V^{5+} 1s−3d transition			V^{4+} 1s−3d transition			
catalyst	gas[a]	height	fwhm (eV)	position (eV)	height	fwhm (eV)	position (eV)	χ^2
PV0.99	O_2/He	0.475	2.6	5470.9				0.090
PV0.99	He/O_2/C_4H_{10}	0.442	2.6	5470.9	0.095	2.6	5469.4	0.067
PV1.95	O_2/He	0.115	2.6	5470.9	0.319	3.2	5469.3	0.061
PV1.95	He/O_2/C_4H_{10}	0.041	2.6	5470.9	0.362	3.5	5469.2	0.061

[a] 20% O_2 in He or 89% He/10% O_2/1%C_4H_{10}.

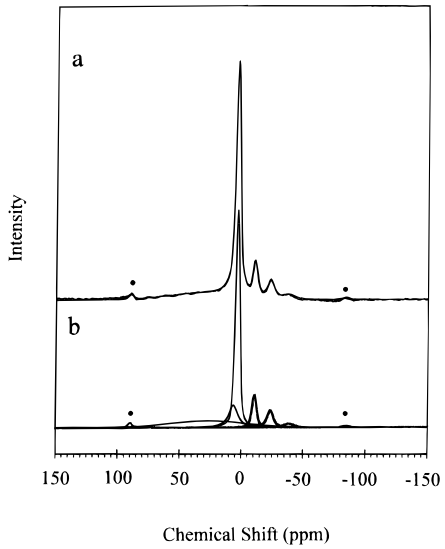

Figure 6. ^{31}P MAS NMR spectrum of reaction-used PV0.95: (a) collected and fitted spectra and (b) deconvoluted peaks. Marked peaks are spin side bands.

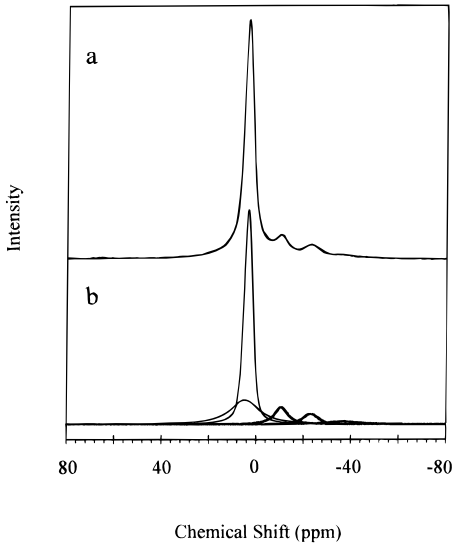

Figure 7. ^{31}P MAS NMR spectrum of reaction-used PV0.95 that was treated in O_2 at 310 °C for 3 h: (a) collected and fitted spectra and (b) deconvoluted peaks.

TABLE 4: Parameters Used to Fit the ^{31}P MAS NMR Spectrum of Reaction-Used PV0.95 Sample

center (ppm)	height	width (ppm)	% Lorentzian	peak area (arb unit)
27.1	5	75	1	410
6.4	18	9	100	234
3.5	170	4	40	902
−10.5	25	4	53	147
−23.4	13	6	81	120
−38.6	3	11	13	34

TABLE 5: Parameters Used to Fit the ^{31}P MAS NMR Spectrum of Reaction-Used and Reoxidized PV0.95

center (ppm)	height	width (ppm)	% Lorentzian	peak area (arb unit)
4.7	29	15	44	626
3.5	260	4	92	1446
−10.6	21	7	100	211
−23.1	13	8	51	125
−36.5	3	18	100	89

with a dominant species with a structure similar to α_1-$VOPO_4$. This species undergoes hydration to and dehydration from $VOPO_4 \cdot 2H_2O$ reversibly. However, the ^{31}P MAS NMR data also demonstrate that only about 77% of the P present is associated with V. The rest exists as P/SiO_2. It is possible that only a portion of the V in the sample is associated with P in the compound α_1-$VOPO_4$, and the remaining portion is present as V/SiO_2, which is known to have poor selectivity for maleic anhydride.[32] However, there is no evidence in the Raman spectra of isolated vanadyl species or V_2O_5 crystallites. Nonetheless, this possibility cannot be excluded. Alternatively, all of the vanadium in the sample can be associated with P to form a compound with $V_{1.1}P_{0.9}O_5$ stoichiometry. Jordan and Calvo[33] have reported a crystal structure for a phosphorus deficient analogue to α_1-$VOPO_4$, α_{II}-$V_{1.1}P_{0.9}O_5$. In this material, 10% of the vanadium occupies the phosphorus tetrahedral sites. The α_1-$VOPO_4$ and α_{II}-$VOPO_4$ phases are closely related. Tachez and co-workers have proposed that the two polymorphs are identical except for the positions of the vanadyl bonds relative to the neighboring phosphate groups. In both structures, chains of distorted vanadia octahedra with alternating long and short vanadyl bonds are linked through corner-sharing phosphate tetrahedra.[34] Tachez and co-workers proposed that the α_1-$VOPO_4$ material has the vanadyl bonds on the same side of the octahedral equatorial plane as the phosphate tetrahedra, whereas in the α_{II}-$VOPO_4$ phase they are on opposite sides. Therefore, it seems reasonable that the α_1 structure should also be able to stabilize a certain fraction of the vanadium in the phosphorus sites. Indeed, the PV0.99 sample undergoes hydration to and dehydration from $VOPO_4 \cdot 2H_2O$ as readily as α_1-$VOPO_4$ and has a selectivity for maleic anhydride similar to that of α_1-$VOPO_4$.[35,36]

The $V_{1.1}P_{0.9}O_5$ material contains only one crystallographically unique phosphorus site. The phosphate groups are corner-sharing with distorted VO_6 octahedra. Substitution of one phosphorus atom with a V atom at the tetrahedral site could change the local environment of the surrounding symmetry-related phosphate groups, thereby weakening the total bond strength at the phosphate atoms sufficiently to produce a slightly different NMR shift.[31] This might be the origin of the 6.4 ppm ^{31}P MAS NMR peak.

Thus, the current data confirm the conclusion in our earlier paper that supported samples of P/V = 1 reported in the literature do not contain $(VO)_2P_2O_7$ but instead $VOPO_4$ materials which are responsible for the poor maleic anhydride selectivities.[11]

PV2 Samples. The data are less clear as to the structure of the VPO species in sample PV1.95. XRD only detects diffraction from a structure similar to α_1-$VOPO_4$, and Raman

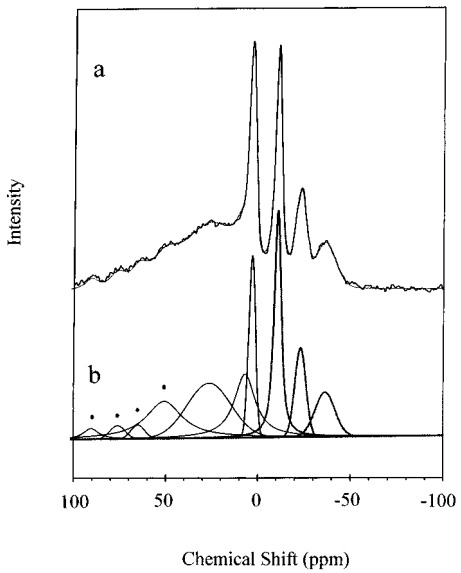

Figure 8. ^{31}P MAS NMR spectrum of reaction-used PV1.95: (a) collected and fitted spectra and (b) deconvoluted peaks. Marked peaks are spin side bands.

TABLE 6: Parameters Used to Fit the ^{31}P MAS NMR Spectrum of Reaction-Used PV1.95

center (ppm)	height	width (ppm)	% Lorentzian	peak area (arb unit)
26.3	9	29	1	282
6.9	11	14	100	224
3.2	31	4	1	143
−10.6	39	5	74	253
−23.1	15	7	0	114
−36.4	8	13	7	105

scattering from this species dominates the spectrum. However, both the XANES and ^{31}P MAS NMR results show that a huge majority of the V in this sample exists as V^{4+}. These V^{4+} ions are in a material(s) with insufficient long range order to produce XRD patterns or in a compound(s) with a basic framework similar to that of α_1-$VOPO_4$ but containing mostly V^{4+}.

In the absence of additional evidence, we propose that the sample contains a mixture of at least two VPO species: a poorly crystalline $VO(PO_3)_2$ and a crystalline phase based on the α_1-$VOPO_4$ structure. The possible presence of poorly crystalline $VO(PO_3)_2$ is suggested by the Raman spectrum. For this sample (spectrum 2e), the peaks in the 960−970 cm^{-1} region are more intense, relative to the 930 cm^{-1} peak, than those for α_1-$VOPO_4$ (spectrum 2b). $VO(PO_3)_2$ has a Raman peak at about 961 cm^{-1}, which can be very weak for a poorly crystalline sample.[27] This compound has a P/V ratio of 2, a vanadium valence of 4.0, and has been shown to have high selectivity for maleic anhydride, albeit low activity.[27]

The XRD pattern can be explained by a species containing a P/V ratio higher than unity and a structure based on α_1-$VOPO_4$ but with a contraction along the *c* direction to 3.94 Å. The α_1-$VOPO_4$ structure contains tetrahedral holes in between the phosphate groups of adjacent layers (see Figure 9). If we assume that the basic framework remained unaltered, inserting an additional P atom into these tetrahedral holes for every five formula units would produce a $VP_{1.2}O_5$ material. This material would have an average vanadium valence of 4.0. If the "excess" phosphorus did not order, new XRD peaks would not be observed. Instead, diffraction peak intensities would change for peaks with the *hkl* parameters: *hk*0, $h + k = 2n$; *h*00, $h = 2n$; and *hk1*, $h + k = 2n$. The phosphorus coordination environment would be unusual because the interlayer phosphate group would share edges with the two neighboring phosphate tetrahedra to form a $(P_3O_8)^-$ unit. Edge-sharing $P_2S_6^{2-}$ ions have been identified in various salts,[37−39] but small, highly charged cations typically form corner-sharing, not edge-sharing, structures. The relatively weak XRD patterns, coupled with the large XRD background from the silica support, have inhibited efforts to determine whether this sample contains $VP_{1.2}O_5$ as a major component or a minor component mixed with poorly crystalline $VO(PO_3)_2$.

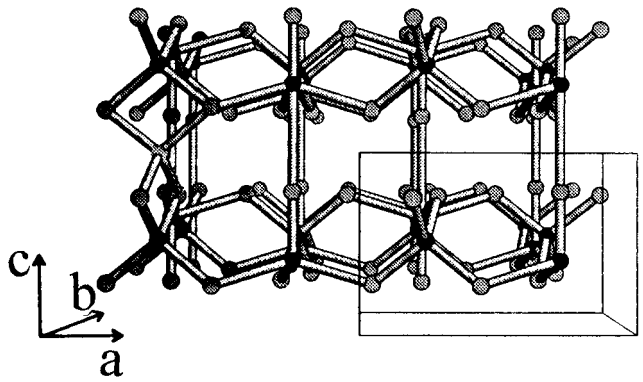

Figure 9. Proposed structure of $VP_{1.2}O_5$.

General Comments. Independent of the structure of the vanadium phosphorus oxide phase in this sample, the data presented here clearly demonstrate the correlation between the stability of the V^{4+} oxidation state and the selectivity for maleic anhydride production in butane oxidation.[1] In another paper we have demonstrated via transient XANES experiments that the presence of V^{5+} in these samples is necessary for maleic anhydride production.[40] The steady-state data presented here are consistent with the concept that the rate of the metal ions at an active site to undergo redox determines the number of oxygen atoms (ions) available to react with a surface hydrocarbon intermediate, which in turn determines selectivity.[41] Materials containing high V^{5+} concentrations under steady-state conditions, therefore, promote overoxidation to combustion products.

The data also show a strong support effect on the formation of the VPO phases. A preparation method that would result in the formation of unsupported vanadyl pyrophosphate did not produce this compound in the presence of silica. Instead, the crystalline phase formed had a structure similar to α_1-$VOPO_4$ preferentially. This phenomenon occurred over a wide range of P/V ratios. At present, we believe that the interaction of silica with V and P changes the energetics of the crystallization process, such that the formation of vanadyl pyrophosphate is no longer favorable. If this interaction is reduced, such as by using a hydrophobic support, formation of VPO phases other than α_1-$VOPO_4$ may become possible. This is being investigated, and the results will be reported in the future.

Conclusion

In this study, it is confirmed that the selectivity for maleic anhydride in butane oxidation depends strongly on the P/V ratio in a SiO_2-supported VPO catalyst, over the range of P/V from 0 to about 2. The presence of SiO_2 strongly affects the crystallization behavior of VPO, effectively hindering the formation of $(VO)_2P_2O_7$ under conditions where it would be formed in the absence of the support. In both the supported $P/V = 1$ and $P/V = 2$ samples, the predominant crystalline phase detectable by X-ray diffraction and Raman scattering is α_1-$VOPO_4$ or a phase very similar to it, although substitution of V into some P sites might occur. For the PV2 sample, the data suggest the possible presence of another phase with stable V^{4+}.

However, conclusive identification of this phase is not possible with the data, although $VO(PO_3)_2$ is a possibility.

Acknowledgment. Support by the U.S. Department of Energy, Basic Energy Sciences, Chemical Sciences Division, helpful discussions with Prof. M. C. Kung, and experimental assistance from Dr. Peter I. Lee are acknowledged. The XANES measurements were performed at the NSLS Brookhaven National Laboratory, which is supported by DOE under contract DC-AC02-76CH00016.

Supporting Information Available: Plot depicting selectivity as a function of butane conversion, XRD patterns for PV0.99 and PV1.95, and ^{31}P MAS NMR spectra of a 0.83 wt % P/SiO_2 sample (5 pages). Ordering information is given on any current masthead page.

References and Notes

(1) Centi, G.; Trifiró, F.; Ebner, J. R.; Franchetti, V. M. *Chem. Rev.* **1988**, *88*, 55.
(2) Cavani, F.; Centi, G.; Tifiro, F. *Appl. Catal.* **1984**, *9*, 191.
(3) Horowitz, H. S.; Blackstone, C. M.; Sleight, A. W.; Teufer, G. *Appl. Catal.* **1988**, *38*, 193.
(4) Garbassi, F.; Bart, J.; Tassinari, R.; Vlaic, G.; Labard, P. *J. Catal.* **1986**, *98*, 317.
(5) Batis, N. H.; Batis, H.; Ghorbel, A.; Vedrine, J. C.; Volta, J.-C. *J. Catal.* **1991**, *128*, 248.
(6) Satsumi, A. J.; Hattori, A.; Furuta, A.; Miyamoto, A.; Hattori, T.; Murakami, Y. *J. Phys. Chem.* **1988**, *92*, 2275.
(7) Zhang, Y.; Sneeden, R. P. A.; Volta, J.-C. *Catal. Today* **1993**, *16*, 39.
(8) Cornaglia, L. M.; Lombardo, E. A. *Appl. Catal. A* **1995**, *127*, 125.
(9) Coulston, G. W.; Thompson, E. A.; Herron, N. *J. Catal.* **1996**, *163*, 122.
(10) Okuhara, T.; Nakama, T.; Misono, M. *Chem. Lett.* **1990**, 1941.
(11) Harding, W. D.; Birkeland, K. E.; Kung, H. H. *Catal. Lett.* **1994**, *28*, 1.
(12) Harding, W. D., Ph.D. thesis, Northwestern University, 1993.
(13) Birkeland, K. E., Ph.D. thesis, Northwestern University, 1995.
(14) Zazhigalov, V. A.; Zaitsev, Y. P.; Belousor, V. M.; Parlitz, B.; Hanke, W.; Öhlman, G. *React. Kinet. Catal. Lett.* **1986**, *32*, 209.
(15) Martinez-Lara, M.; Moreno-Real, L.; Pozas-Tormo, R.; Jimenez-Lopez, A.; Bruque, S.; Ruiz, P.; Poncelet, G. *Can. J. Chem.* **1992**, *70*, 5.
(16) Do, N. T.; Baerns, M. *Appl. Catal.* **1988**, *45*, 1; **1988**, *45*, 9.
(17) Martinez-Lara, M.; Jimenez-Lopez, A.; Moreno-Real, L. *Mater. Res. Bull.* **1986**, *21*, 13.
(18) Ladwig, V. G. *Z. Anorg. Allg. Chem.* **1965**, *338*, 266.
(19) Sananes, M. T.; Hutchings, G. J.; Volta, J.-C. *J. Chem. Soc., Chem. Commun.* **1995**, 243.
(20) Busca, G.; Centi, G.; Trifiró, F.; Lorenzelli, V. *J. Phys. Chem.* **1986**, *90*, 1337.
(21) Andersen, P. J.; Kung, H. H. *J. Phys. Chem.* **1992**, *96*, 3114.
(22) Lee, P. L.; Beno, M. A.; Jennings, G.; Ramanathan, M.; Knapp, G. S.; Huang, K.; Bai, J.; Montano, P. A. *Rev. Sci. Instrum.* **1994**, *65*, 1.
(23) Lytle, F. W.; Greegor, R. B.; Marques, E. C.; Sandstrom, D. R.; Via, G. H. Sinfelt, J. H. *J. Catal.* **1985**, *95*, 546.
(24) Furenlid, L.; Bouldin, C.; Elam, T. Unpublished results.
(25) Benabdelouahab, F.; Olier, R.; Guilhaume, N.; Lefebvre, F.; Volta, J.-C. *J. Catal.* **1992**, *134*, 151.
(26) Benabdelouahab, F.; Volta, J.-C.; Olier, R. *J. Catal.* **1994**, *148*, 334.
(27) Sananes, M. T.; Hutchings, G. J.; Volta, J.-C. *J. Catal.* **1995**, *154*, 253.
(28) Wong, J.; Lytle, F. W.; Messmer, R. P.; Maylotte, D. H. *Phys. Rev. B* **1984**, *30*, 5596.
(29) Szu, S.-P.; Klein, L. C.; Greenblatt, M. *J. Non-Cryst. Solids* **1992**, *143*, 21.
(30) Ennaciri, S. A.; R'Kha, C.; Bardoux, P.; Livage, J. *Eur. J. Solid State Inorg. Chem.* **1993**, *30*, 227.
(31) Cheetham, A. K.; Nigel, J. C.; Dobson, C. M.; Jakeman, J. B. *J. Chem. Soc., Chem. Commun.* 1986, 195.
(32) Owens, L.; Kung, H. H. *J. Catal.* **1993**, *144*, 202.
(33) Jordan, B. D.; Calvo, C. *Acta Crystallogr.* **1976**, *B32*, 2899.
(34) Tachez, M.; Theobald, F.; Bordes, E. *J. Solid State Chem.* **1981**, *40*, 280.
(35) Shimoda, T.; Okuhara, T.; Misono, M. *Bull. Chem. Soc. Jpn.* **1985**, *58*, 2163.
(36) Takita, Y.; Hashiguchi, T.; Matsunosako, H. *Bull. Chem. Soc. Jpn.* **1988**, *61*, 3737.
(37) Toffoli, P. P.; Khodadad, P.; Rodier, N. *Acta Crystallogr.* **1978**, *B34*, 3561.
(38) Nitsche, R.; Wild, P. *Mater. Res. Bull.* **1970**, *5*, 419.
(39) Bouchetière, M.; Toffoli, P. P.; Khodada, P.; Rodier, N. *Acta Crystallogr.* **1978**, *B34*, 384.
(40) Coulston, G. W.; Bare, S. R.; Kung, H. H.; Birkeland, K.; Bethke, G. K.; Harlow, R.; Lee, P. L. *Science* **1997**, *275*, 191.
(41) Kung, H. H. *Adv. Catal.* **1994**, *40*, 1.